

Simulation of Nonlinear Contaminant Transport
in Groundwater by a Higher Order
Godunov-Mixed Finite Element Method

Clint N. Dawson

April, 1991

TR91-06

Simulation of Nonlinear Contaminant Transport in Groundwater by a Higher Order Godunov-Mixed Finite Element Method

Clint Dawson

*Department of Mathematical Sciences, Rice University, Houston, Texas
77251 U.S.A.*

Abstract: We consider the numerical simulation of contaminant transport in groundwater where the mathematical model includes a nonlinear adsorption term. The method we describe combines a higher order Godunov scheme for advection with a mixed finite element method for diffusion. The method is formulated in one space dimension, and numerical results for equilibrium and nonequilibrium adsorption are presented.

1 Introduction

As noted in two recent reports by the Environmental Protection Agency and the Department of Energy, the quality of groundwater at many locations in the United States is being threatened by the introduction of hazardous chemicals into the subsurface [1, 2]. Such chemicals include hydrocarbons, herbicides, and pesticides. In areas where groundwater is a major source of drinking water, such contamination poses a threat to the public health.

Modeling the flow of hazardous chemicals through the subsurface has seen increasing interest in recent years. The mathematical models which describe contaminant flow include terms which account for the aquifer characteristics (hydraulic conductivity, porosity, etc.), the presence of microorganisms capable of biodegrading certain compounds, and adsorption. Biodegradation is an important aspect of contaminant flow, as many compounds may be eliminated by natural biodegradation. Moreover, natural biodegradation processes may be enhanced to effectively remove contaminants [1]. Adsorption, which is a retardation/release reaction between the solute and the surface of the porous structure, is also a significant factor in contaminant movement. Adsorption can have the effects of segregating a hazardous compound from the groundwater, and slowing the overall movement of the compound.

In many cases contaminants are introduced to an aquifer through the unsaturated zone. A complete mathematical and numerical treatment of contaminant transport would include both the unsaturated and saturated zones. In this case,

under certain simplifying assumptions, the mathematical description of the problem involves an elliptic/parabolic partial differential equation for pressure head, and a parabolic equation describing transport of contaminant. We will present a model which takes into account both the saturated and unsaturated regions. Numerically, we will focus on an algorithm for the transport equation only.

The author and M. F. Wheeler have developed and tested an algorithm for modeling multidimensional, multicomponent flow in the saturated zone which includes the effects of biodegradation and linear adsorption, see for example [3, 4]. In this code, a finite element modified method of characteristics models advection, and a mixed finite element method is used to calculate head and velocity. Nonlinear reaction terms modeling biodegradation are incorporated into the algorithm by time-splitting. In this paper, we consider the application of higher-order Godunov-mixed finite element methods to similar problems; however, we want to incorporate the effects of (possibly) nonlinear adsorption. Nonlinear adsorption complicates the model by the inclusion of a nonlinear time derivative and/or source term(s). In an earlier paper [5], the author and M. F. Wheeler described a first-order method for simulating these types of problems. Here, we describe a higher-order extension of this technique and use it to study nonlinear adsorption phenomena.

2 Problem Description

In saturated flow, the flow velocity \mathbf{u} (L/T) of water satisfies Darcy's Law:

$$\mathbf{u} = -K\nabla h, \quad (1)$$

where K (L/T) is hydraulic conductivity and h (L) is the piezometric head. K is given by

$$K = \frac{k\gamma}{\mu}, \quad (2)$$

where k is the permeability of the medium and is possibly spatially dependent, γ is the specific weight of water, and μ is water viscosity.

In the unsaturated zone, where both air and water are present, if we assume air is stagnant and at a constant pressure, then

$$\mathbf{u} = -K(\Psi)\nabla h, \quad (3)$$

where in this case

$$K = \frac{kk_{rw}(\Psi)\gamma}{\mu}.$$

Here, $k_{rw}(\Psi)$ is the relative permeability of water, which is assumed to be a function of pressure head Ψ (L). The piezometric head is related to pressure head by

$$h = z + \Psi. \quad (4)$$

where z is the elevation of the water table. In the saturated zone, $\Psi \geq 0$, and in the unsaturated zone, $\Psi < 0$. If we extend the definition of $k_{rw}(\Psi)$ by $k_{rw}(\Psi) \equiv 1$ for $\Psi > 0$, then (3) is valid in both zones.

Let θ denote water content, which is a function of Ψ . In the saturated zone, $\theta(\Psi) \equiv \phi$, where ϕ is porosity. In the unsaturated zone, $0 < \theta < \phi$. Between these two zones lies the capillary fringe, or tension-saturated zone, where the functional relationship $\theta(\Psi)$ is soil-dependent. Water content and the flow velocity are related by

$$\theta_t + \nabla \cdot \mathbf{u} = q(x, t), \quad (5)$$

where $q(x, t)$ models source and sink terms. Thus, in the unsaturated zone, substituting (3) into (5), we obtain a nonlinear differential equation in Ψ , and in the saturated zone,

$$\nabla \cdot \mathbf{u} = -\nabla \cdot (K \nabla h) = q(x, t). \quad (6)$$

Thus, (5) is parabolic in the unsaturated zone, and elliptic in the saturated zone.

For more discussion on the saturated and unsaturated zones, and the capillary fringe, see [6] and [7].

Let c denote the concentration of some chemical species, which we will assume is soluble with water. Solute transport is described by [7]

$$(\theta c)_t + \rho A_t + \nabla \cdot (\mathbf{u}c - \theta D \nabla c) = r(x, c, t), \quad (7)$$

Here D (L^2/T) denotes the sum of the molecular diffusion and mechanical dispersion coefficients, and r is a source term, which could include point sources and sinks. The term ρA represents the amount of solute adsorbed, where ρ (M/V) is the bulk density.

In many cases of physical interest, flow is advection-dominated; that is, \mathbf{u} is much "larger" than D , appropriately scaled. It is well known that standard finite element and finite difference techniques do not work well for these types of problems. However, the method we discuss here is capable of resolving sharp fronts without oscillation and with minimal numerical diffusion.

The term ρA is in general heterogeneous, depending on the adsorbent surfaces. The adsorption process can be divided into two classes, equilibrium and non-equilibrium. Adsorption is assumed to be in equilibrium when the reaction kinetics occur at a much faster rate than the rate of transport. A can be expressed as [8]

$$A = \lambda_1 \psi(c) + \lambda_2 s, \quad (8)$$

where $\lambda_i \geq 0$, $i = 1, 2$, and $\lambda_1 + \lambda_2 = 1$; $\psi(c)$ describes adsorption at equilibrium sites, and s describes adsorption at non-equilibrium sites. The latter term is assumed to satisfy

$$s_t = k_d \Phi(c) - k_s s, \quad (9)$$

where k_a ($1/T$) and k_s ($1/T$) are nonnegative constants. The functions $\psi(c)$ and $\Phi(c)$ are adsorption isotherms. Two common isotherms are the Langmuir isotherm, :

$$f_L(c) = \frac{K_d c}{1 + K_2 c}, \quad (10)$$

where K_d (V/M) and $K_2 > 0$, and the Freundlich isotherm,

$$f_F(c) = K_d c^p, \quad 0 < p \leq 1, \quad (11)$$

Note that $f_F(c)$ is not Lipschitz continuous at $c = 0$ for $0 < p < 1$.

3 A Numerical method for transport

For the purposes of discussing a numerical method for the transport equation (7), we assume water content θ and velocity \mathbf{u} are given. For simplicity, we will assume saturated flow, thus $\theta \equiv \phi$. We are interested primarily in the effects of nonlinear adsorption. Thus, to ease the presentation, we reduce the problem to one space dimension, and assume no source terms are present in either (6) or (7). In this case, the flow velocity \mathbf{u} becomes a scalar constant u .

First, consider the case of adsorption in equilibrium; i.e., $\lambda_1 = 1$ and $\lambda_2 = 0$ in (8). We assume $u > 0$ and prescribe an inflow concentration $c = c_0$ at $x = 0$. Equation (7) reduces to

$$c_t + \bar{\rho}\psi(c)_t + \bar{u}c_x - Dc_{xx} = 0, \quad x > 0, \quad t > 0, \quad (12)$$

where $\bar{\rho} = \rho/\phi$, $\bar{u} = u/\phi$, and ψ is either the Freundlich or Langmuir isotherm. We assume initially that $c(x, 0) = c^0(x)$.

Let $\mu = c + \bar{\rho}\psi(c)$. Then $\mu(c)$ is a continuous, one-to-one, and onto mapping from $[0, \infty) \rightarrow [0, \infty)$. Thus, the inverse of μ , $\eta(\mu) = c$, exists, and (12) can be written as a parabolic equation (possibly degenerate) in μ :

$$\mu_t + \bar{u}\eta(\mu)_x - D\eta(\mu)_{xx} = 0, \quad x > 0, \quad t > 0. \quad (13)$$

As mentioned earlier, if $\psi(c)$ is given by the Freundlich isotherm, with $0 < p < 1$, we encounter the difficulty that the nonlinearity c^p is non-Lipschitz at $c = 0$. Moreover, flow is generally advection-dominated, thus the solution exhibits sharp fronts. The effects of choosing $p < 1$ (as opposed to $p = 1$) are to make the fronts even sharper, and to further retard the flow of the chemical species. In fact, in the limit of zero diffusion with $p < 1$, solutions to (13) can exhibit shocks for smooth initial data.

For advection-dominated flow problems similar to (13), we have studied the application of higher-order Godunov-mixed methods (GMM). This class of methods was formulated and analyzed for nonlinear advection-diffusion equations in

[9]. A multidimensional extension of the method is described in [10]. We now describe the application of this algorithm to (13).

Assume the computational domain is truncated to a region $(0, \bar{x})$. At the point \bar{x} assume the “outflow” condition

$$\mu_t + \bar{u}\eta(\mu)_x = 0, \quad \text{at } x = \bar{x}. \quad (14)$$

Let $0 = x_{1/2} < x_{3/2} < \dots < x_{J+1/2} = \bar{x}$ be a partition of $[0, \bar{x}]$ into grid blocks $B_j = [x_{j-1/2}, x_{j+1/2}]$, and let x_j be the midpoint of B_j , $h_j = x_{j+1/2} - x_{j-1/2}$, and $h_{j+1/2} = (h_j + h_{j+1})/2$. Let $\Delta t > 0$ denote a time-stepping parameter, and let $t^n = n\Delta t$. For functions $g(x, t)$, let $g_j^n = g(x_j, t^n)$.

On each grid block B_j , approximate μ^n by a piecewise linear function w^n , where

$$w^n|_{B_j} = w_j^n + (x - x_j)\delta w_j^n, \quad j = 1, \dots, J; \quad (15)$$

c^n is approximated by a piecewise constant function C^n , where

$$C^n|_{B_j} = C_j^n. \quad (16)$$

In (15),

$$w_j^n \equiv C_j^n + \bar{\rho}\psi(C_j^n). \quad (17)$$

Initially, set $C_j^0 = c^0(x_j)$, $j = 1, \dots, J$. Assume for some time level t^n the approximate solution C^n is known. The GMM is based on splitting (13) into an advection equation:

$$\bar{\mu}_t + \bar{u}\eta(\bar{\mu})_x = 0, \quad x > 0, \quad t \in (t^n, t^{n+1}), \quad (18)$$

and a diffusion equation

$$\mu_t^* - D\eta(\mu^*)_{xx} = 0, \quad x > 0, \quad t \in (t^n, t^{n+1}). \quad (19)$$

Taking C^n as the initial condition, we apply a higher-order Godunov (HOG) scheme to (18). The solution generated from this step then serves as the initial condition for (19), where a mixed finite element method (MFEM) is applied. The result of these two steps is an approximation, C^{n+1} , to the solution at time t^{n+1} .

Let \bar{w}^{n+1} be the HOG solution to (18) at time t^{n+1} . The HOG approach we will consider is similar to the MUSCL scheme proposed by van Leer [11]. Integrate (18) over the region $B_j \times [t^n, t^{n+1}]$ and apply the midpoint rule in time to obtain

$$\bar{w}_j^{n+1} = w_j^n - \frac{\Delta t}{h_j} \left[\eta(\bar{w}_{j+1/2}^{n+1/2}) - \eta(\bar{w}_{j-1/2}^{n+1/2}) \right], \quad (20)$$

where $\bar{w}_j^{n+1} = \bar{w}^{n+1}|_{B_j}$.

The term $\eta(\bar{w}_{j+1/2}^{n+1/2})$ is an approximation to $\eta(\mu(x_{j+1/2}, t^{n+1/2}))$, and represents the advective flux across a grid block boundary. At the inflow boundary,

$$\eta(\bar{w}_{1/2}^{n+1/2}) = c_0^{n+1/2}.$$

At the other grid block boundaries, this term is approximated by characteristic tracing from the point $(x_{j+1/2}, t^{n+1/2})$ back to time t^n . Define the characteristics $x_L(t)$ and $x_R(t)$ satisfying

$$x_L'(t) = \max(0, \bar{u}\eta'(w_j^n)), \quad x_L(t^{n+1/2}) = x_{j+1/2}, \quad (21)$$

and

$$x_R'(t) = \min(0, \bar{u}\eta'(w_{j+1}^n)), \quad x_R(t^{n+1/2}) = x_{j+1/2}. \quad (22)$$

Let cfl be a specified parameter, $0 < cfl \leq 1$. Assuming the CFL constraint

$$\lambda_j^n = \frac{\Delta t}{h_j} \bar{u}\eta'(w_j^n) \leq cfl \leq 1, \quad j = 1, \dots, J, \quad (23)$$

then $x_L(t)$ crosses the $t = t^n$ axis at a point $x_{j,L}$, where $x_{j,L} \in B_j$, and $x_R(t)$ crosses at a point $x_{j,R} \in B_{j+1}$. In general, $\eta(\bar{w}_{j+1/2}^{n+1/2})$ is determined by upwinding; i.e., we evaluate η at $x_{j,L}$ or $x_{j,R}$, depending on the local direction of flow. Since we are assuming $\bar{u} > 0$, and since

$$\eta'(\mu(c)) = \frac{1}{\mu'(c)} \geq 0, \quad c \geq 0,$$

we find that

$$x_{j,L} = x_{j+1/2} - \frac{\Delta t}{2} \bar{u}\eta'(w_j^n), \quad (24)$$

and

$$\eta(\bar{w}_{j+1/2}^{n+1/2}) \equiv \eta(w^n(x_{j,L})). \quad (25)$$

The diffusion equation, (19), is handled using the MFEM with the lowest order Raviart-Thomas approximating spaces [12]. In [13], it is shown that this scheme, with the appropriate quadrature rule, is equivalent to block centered finite differences applied to (19). Let $\gamma(x, t)$ denote the diffusive flux,

$$\gamma(x, t) = -D\eta(\mu(x, t))_x = -Dc_x(x, t). \quad (26)$$

Using block centered finite differences in (26), $\gamma(x_{j+1/2}, t^n)$ is approximated by $\bar{\gamma}_{j+1/2}^n$, where

$$\bar{\gamma}_{j+1/2}^n = -D \frac{C_{j+1}^n - C_j^n}{h_{j+1/2}}, \quad j = 1, \dots, J-1. \quad (27)$$

At the inflow boundary,

$$\bar{\gamma}_{1/2}^n = -2D \frac{C_1^n - c_0^n}{h_1}. \quad (28)$$

We discuss the handling of the outflow boundary condition (14) below.

Discretizing (19) using backward differencing in time and block centered differencing in space, and taking \bar{w}^{n+1} as the initial condition, we obtain

$$\frac{w_j^{n+1} - \bar{w}_j^{n+1}}{\Delta t} + \frac{\bar{\gamma}_{j+1/2}^{n+1} - \bar{\gamma}_{j-1/2}^{n+1}}{h_j} = 0, \quad (29)$$

which holds for $j = 1, \dots, J-1$. Substitute for \bar{w}_j^{n+1} using (20) to obtain

$$\frac{w_j^{n+1} - w_j^n}{\Delta t} + \frac{\eta(\bar{w}_{j+1/2}^{n+1/2}) - \eta(\bar{w}_{j-1/2}^{n+1/2})}{h_j} + \frac{\bar{\gamma}_{j+1/2}^{n+1} - \bar{\gamma}_{j-1/2}^{n+1}}{h_j} = 0. \quad (30)$$

In block B_J , first compute \bar{w}_J^{n+1} by

$$\frac{\bar{w}_J^{n+1} - w_J^n}{\Delta t} + \bar{u} \frac{\eta(\bar{w}_{J+1/2}^{n+1/2}) - \eta(\bar{w}_{J-1/2}^{n+1/2})}{h_J} = 0. \quad (31)$$

Set $C^{n+1}(\bar{x}) = \eta(\bar{w}_J^{n+1})$, and approximate the diffusive flux at \bar{x} by

$$\bar{\gamma}_{J+1/2}^{n+1} = -2D \frac{C^{n+1}(\bar{x}) - C_J^{n+1}}{h_J}. \quad (32)$$

Then w_j^{n+1} is given by (30).

Substituting (17), (25), (27), (28), and (32) into (30), we obtain a tridiagonal system of equations for C_j^{n+1} , $j = 1, \dots, J$, which is possibly nonlinear. Once C_j^{n+1} is determined, w_j^{n+1} is updated by (17).

The last step in the calculation at time t^{n+1} is the computing of the slopes, δw_j^{n+1} , $j = 1, \dots, J$, which only appear in the characteristic tracing step. The slope in the last interval, δw_J^{n+1} is set to zero. In the remaining intervals, set

$$\delta w_j^{n+1} = \delta_{lim} w_j^{n+1} \cdot \text{sign}(w_{j+1}^{n+1} - w_{j-1}^{n+1}), \quad (33)$$

where

$$\delta_{lim} w_j^{n+1} = \begin{cases} \min(|\Delta_+ w_j^{n+1}|, |\Delta_- w_j^{n+1}|), & \text{if } \Delta_+ w_j^{n+1} \cdot \Delta_- w_j^{n+1} > 0, \\ 0, & \text{otherwise.} \end{cases} \quad (34)$$

Here $\Delta_+ w_j$ is the forward difference $(w_{j+1} - w_j)/h_{j+1/2}$. For $j = 2, \dots, J-1$, $\Delta_- w_j = (w_j - w_{j-1})/h_{j-1/2}$, and $\Delta_- w_1 = 2(w_1 - c_0)/h_1$. The point of the procedure (33)-(34) is to compute a piecewise linear approximation without

introducing new extrema into the approximate solution. Thus, in blocks where the solution already has a local extrema, the slope δw_j^{n+1} is set to zero.

Assuming

$$cfl \leq \frac{1}{1 + \frac{\alpha_l}{2}},$$

where

$$\alpha_l = \max_j \frac{h_j}{h_{j-1/2}},$$

the techniques given in [9] can be extended to prove that the approximate solution C^{n+1} defined above satisfies a maximum principle; that is,

$$\min \left(c_0, \min_j c^0(x_j) \right) \leq C_j^{n+1} \leq \max \left(c_0, \max_j c^0(x_j) \right). \quad (35)$$

Moreover, assuming linear, equilibrium adsorption (Freundlich isotherm, $p = 1$), and assuming a Dirichlet boundary condition is given at \bar{x} , then, for c sufficiently smooth, one can prove [9],

$$\max_n \left(\sum_j [c_j^n - C_j^n]^2 h_j \right)^{1/2} \leq C(h + \Delta t), \quad (36)$$

where $h = \max_j h_j$. This pessimistic estimate says the scheme is at worst first order accurate. However, the accuracy depends on the number of local extrema in the approximate solution, that is, the number of times $\delta_{lim} w_j$ is set to zero in areas where $\mu_x \neq 0$. Heuristically, one expects this number to be small, in which case the error approaches $\mathcal{O}(h^2 + \Delta t)$. Numerical studies which verify this heuristic notion are given in [9]. In practice, we see much better performance from the scheme outlined above than from standard first-order schemes.

We can modify the definition of $\delta_{lim} w_j^{n+1}$ by

$$\delta_{lim} w_j^{n+1} = \min(|\Delta_+ w_j^{n+1}|, |\Delta_- w_j^{n+1}|). \quad (37)$$

In this case, one can prove that

$$\max_n \left(\sum_j [c_j^n - C_j^n]^2 h_j \right)^{1/2} \leq C(h^2 + \Delta t); \quad (38)$$

however, (35) is no longer guaranteed to hold.

Remarks on simulating non-equilibrium adsorption. Assume $\lambda_1 = 0$ and $\lambda_2 = 1$, then we obtain the system of equations

$$c_t + \bar{u}c_x - Dc_{xx} = -\rho(k_a\Phi(c) - k_s s) \equiv g(c, s), \quad (39)$$

$$s_t = k_a \Phi(c) - k_s s. \quad (40)$$

We discretize (39) as before, incorporating the source term $g(c, s)$ implicitly. We also apply an implicit discretization to (40). Thus at each time t^{n+1} , we have an implicit system of equations in $C^{n+1} \approx c^{n+1}$, and $S^{n+1} \approx s^{n+1}$. In this case, C^{n+1} is piecewise linear in space, and S^{n+1} is piecewise constant.

4 Numerical results

In this section, we present numerical results for both equilibrium and non-equilibrium adsorption assuming the adsorption kinetics is described by the Freundlich isotherm, (11). In particular, we will examine the effects of varying the exponent p .

We first consider the case of equilibrium adsorption; $\lambda_1 = 1$ and $\lambda_2 = 0$. When $p < 1$, we have a nonlinear tridiagonal system of equations to solve to determine C^{n+1} . We have solved this system numerically using a method of substitution. This approach converges slowly in some cases (especially at early time), but has the advantage that at each iteration, the approximate solution satisfies a maximum principle. Thus, we are guaranteed that the solution values stay nonnegative, which is crucial to the iteration, since c^p is undefined for negative c if $p < 1$.

In the simulations described below, we set $c_0 \equiv 1$, $\phi = .5$, $R \equiv \rho K_d / \phi = 1.5$, $u = 3 \text{ cm/h}$, $D = .20 \text{ cm}^2/\text{h}$, and $cf l = 1$. The computational domain is $0 < x \leq 100 \text{ cm}$, and the initial condition $c^0(x)$ is plotted in Figure 1.

We first consider the case $p = .8$. To test the convergence of the scheme, we compare the approximate solutions at $t = 20$ hours, generated using 25, 50, and 100 uniform grid blocks. As seen in Figure 1, the numerical solution appears to converge as the mesh and time step approach zero. This figure also shows the effect of choosing $p < 1$. Note that the initial condition has a fairly smooth front, while the solution at $t = 20$ hours has a much steeper front. This effect is not seen when $p = 1$.

In Figure 2, we compare solutions for $p = .5$, $.8$, and 1 at $t = 20$ hours. In these simulations, 100 uniform grid blocks are used. Figure 2 shows that decreasing p results in sharper fronts and substantial retardation of the solution. These results agree with the expected behavior of the solution, based on the mathematical model (12).

Next, we examine the case of non-equilibrium adsorption; $\lambda_1 = 0$ and $\lambda_2 = 1$. For these runs, we assume initially that $c^0(x) = 0$. The values of c_0 , ϕ , u , and D are the same as those given above. We also set $\rho * K_d = 1.5$, and $k_a = k_s = .5$. In Figure 3, we compare the approximations to $c(x, t)$ at $t = 30$ hours, for $p = .5$, obtained using 25, 50, and 100 uniform grid blocks. This figure demonstrates that the approximate solution converges as the mesh and time step are refined.

In Figure 4, we compare solutions at 30 hours for $p = 1$, $.8$, and $.5$. The effects of reducing p in this case are more dramatic than in the equilibrium case.

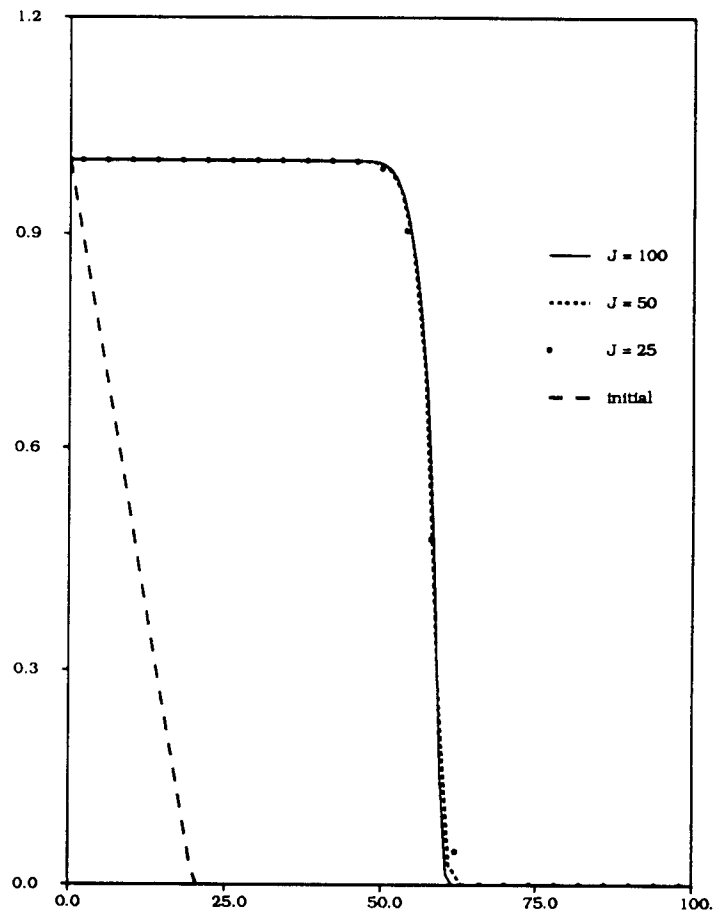


Figure 1: Test of convergence for $p = .8$.

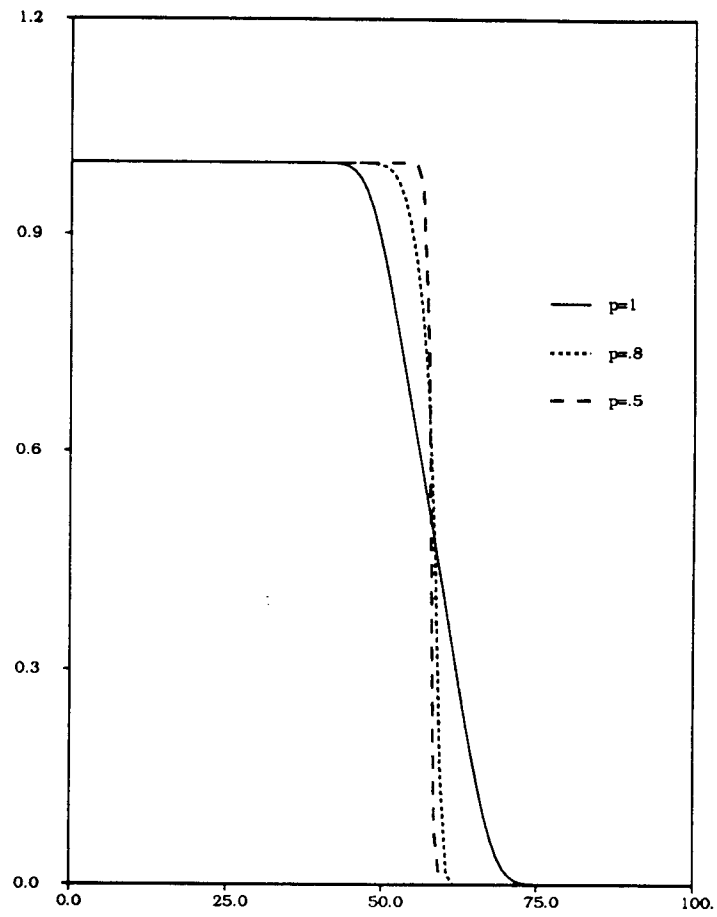


Figure 2: Comparison of $p = .5, .8, \text{ and } 1$.

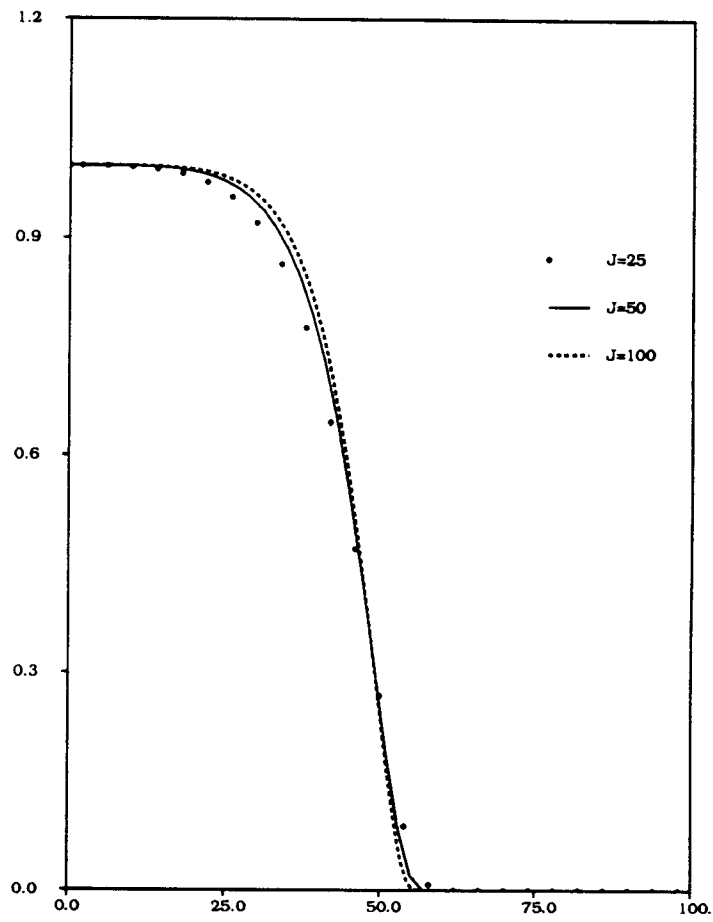


Figure 3: Test of convergence for non-equilibrium case, $p = .5$

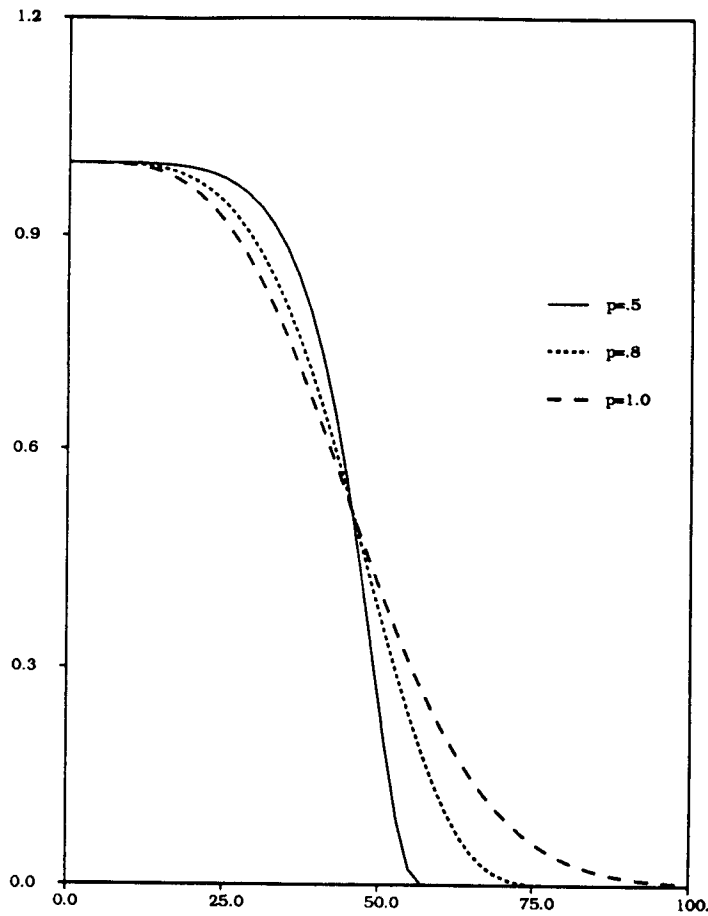


Figure 4: Comparison of $p = .5, .8,$ and $1.,$ nonequilibrium case

Here, the solution for $p = .5$ has a much steeper front and lags substantially behind the $p = 1$ solution, while the $p = .8$ solution is intermediate. Comparing the equilibrium and non-equilibrium solutions, we see that their behavior is quite different. In particular, the solutions in the non-equilibrium case do not have the self-steepening quality that the equilibrium solutions possess (for $p < 1$).

5 Conclusions

In conclusion, the Godunov-mixed method described here gives solutions which agree with physical intuition. The method is convergent, and allows for stable and accurate approximations to contaminant transport problems.

The method has been applied to two case studies of equilibrium and nonequilibrium adsorption in one space dimension. Substantial differences in the numerical results were seen depending on the type of adsorption model chosen.

Thus, the standard assumption of linear, equilibrium adsorption may not be appropriate for some contaminant species.

We have extended the numerical method discussed here to the modeling of two-dimensional, multicomponent saturated transport with biodegradation. At present, biodegradation is modeled by the Monod kinetics, and the method has been tested for three component flow involving a contaminant species, dissolved oxygen, and microorganisms. Some preliminary numerical results have been obtained, and will be presented at a later time.

The two-dimensional simulator uses a mixed finite element method to solve for flow velocity and head. We plan to extend this method to the more general case (5), which models unsaturated and saturated flow. Extending the transport simulator to include variable water content is straightforward. Thus, we hope in the near future to have a simulator capable of modeling contaminant transport through the unsaturated and saturated zones.

References

- [1] J. M. Thomas, M. D. Lee, P. B. Bedient, R. C. Borden, L. W. Canter, and C. H. Ward, *Leaking underground storage tanks: remediation with emphasis on in situ bioremediation*, Environmental Protection Agency, 600/2-87,008, January, 1987.
- [2] United States Department of Energy, *Site-directed subsurface environmental initiative, five year summary and plan for fundamental research in subsoils and in groundwater, FY1989-FY1993*, DOE/ER 034411, Office of Energy Research, April 1988.
- [3] M. F. Wheeler and C. N. Dawson, *An operator-splitting method for advection-diffusion-reaction problems*, MAFELAP Proceedings VI, J. A. Whiteman, ed., Academic Press, pp. 463-482, 1988.
- [4] C. Y. Chiang, C. N. Dawson, and M. F. Wheeler, *Modeling of in-situ bioremediation of organic compounds in groundwater*, to appear in *Transport in Porous Media*.
- [5] C. N. Dawson and M. F. Wheeler, *Characteristic methods for modeling nonlinear adsorption in contaminant transport*, Proceedings, 8th International Conference on Computational Methods in Water Resources, Venice Italy, 1990, Computational Mechanics Publications, Southampton, U. K., pp. 305-314.
- [6] J. Bear, Dynamics of Fluids in Porous Media, Dover Publications, New York, 1972.
- [7] R. A. Freeze and J. A. Cherry, Groundwater, Prentice-Hall, Englewood Cliffs, New Jersey, 1979.

- [8] C. J. van Duijn and P. Knabner, *Solute transport in porous media with equilibrium and non-equilibrium multiple-site adsorption: Travelling waves*, Institut für Mathematik, Universität Augsburg, Report No. 122, 1989.
- [9] C. N. Dawson, *Godunov-mixed methods for advective flow problems in one space dimension*, to appear in SIAM J. Numer. Anal.
- [10] C. N. Dawson, *Godunov-mixed methods for immiscible displacement*, International Journal for Numerical Methods in Fluids 11, pp. 835-847, 1990.
- [11] B. van Leer, *Towards the ultimate conservative difference scheme via a second-order sequel to Godunov's method*, J. Comput. Phys. 32, pp. 101-136, 1979.
- [12] P. A. Raviart and J. M. Thomas, *A mixed finite element method for 2nd order elliptic problems*, in Mathematical Aspects of the Finite Element Method, Rome 1975, Lecture Notes in Mathematics, Springer-Verlag, Berlin, 1977.
- [13] T. F. Russell and M. F. Wheeler, *Finite element and finite difference methods for continuous flow problems*, in The Mathematics of Reservoir Simulation (R. E. Ewing, ed.), Frontiers in Science, SIAM, Philadelphia, 1983.